Syndromic Parkinsonism and Dementia Associated with *OPA1* Missense Mutations

Valerio Carelli, MD, PhD,[1,2] Olimpia Musumeci, MD,[3] Leonardo Caporali, PhD,[1] Claudia Zanna, PhD,[2] Chiara La Morgia, MD, PhD,[1,2] Valentina Del Dotto, PhD,[4] Anna Maria Porcelli, PhD,[4] Michela Rugolo, PhD,[4] Maria Lucia Valentino, MD,[1,2] Luisa Iommarini, PhD,[4] Alessandra Maresca, PhD,[1,2] Piero Barboni, MD,[5] Michele Carbonelli, MD,[5] Costantino Trombetta, MD,[6] Enza Maria Valente, MD, PhD,[7] Simone Patergnani, PhD,[8] Carlotta Giorgi, PhD,[8] Paolo Pinton, PhD,[8] Giovanni Rizzo, MD, PhD,[1,2] Caterina Tonon, MD, PhD,[9] Raffaele Lodi, MD, PhD,[9] Patrizia Avoni, MD, PhD,[1,2] Rocco Liguori, MD,[1,2] Agostino Baruzzi, MD,[1,2] Antonio Toscano, MD,[3] and Massimo Zeviani, MD, PhD[10]

Objective: Mounting evidence links neurodegenerative disorders such as Parkinson disease and Alzheimer disease with mitochondrial dysfunction, and recent emphasis has focused on mitochondrial dynamics and quality control. Mitochondrial dynamics and mtDNA maintenance is another link recently emerged, implicating mutations in the mitochondrial fusion genes *OPA1* and *MFN2* in the pathogenesis of multisystem syndromes characterized by neurodegeneration and accumulation of mtDNA multiple deletions in postmitotic tissues. Here, we report 2 Italian families affected by dominant chronic progressive external ophthalmoplegia (CPEO) complicated by parkinsonism and dementia.

Methods: Patients were extensively studied by optical coherence tomography (OCT) to assess retinal nerve fibers, and underwent muscle and brain magnetic resonance spectroscopy (MRS), and muscle biopsy and fibroblasts were analyzed. Candidate genes were sequenced, and mtDNA was analyzed for rearrangements.

Results: Affected individuals displayed a slowly progressive syndrome characterized by CPEO, mitochondrial myopathy, sensorineural deafness, peripheral neuropathy, parkinsonism, and/or cognitive impairment, in most cases without visual complains, but with subclinical loss of retinal nerve fibers at OCT. Muscle biopsies showed cytochrome c oxidase-negative fibers and mtDNA multiple deletions, and MRS displayed defective oxidative metabolism in muscle and brain. We found 2 heterozygous *OPA1* missense mutations affecting highly conserved amino acid positions (p.G488R, p.A495V) in the guanosine triphosphatase domain, each segregating with affected individuals. Fibroblast studies showed a reduced amount of OPA1 protein with normal mRNA expression, fragmented mitochondria, impaired bioenergetics, increased autophagy and mitophagy.

View this article online at wileyonlinelibrary.com. DOI: 10.1002/ana.24410

Received Jul 14, 2014, and in revised form Mar 23, 2015. Accepted for publication Mar 24, 2015.

Address correspondence to Prof Carelli, IRCCS Institute of Neurological Sciences of Bologna, Bellaria Hospital, Department of Biomedical and NeuroMotor Sciences (DiBiNeM), University of Bologna, Via Altura 3, 40139 Bologna, Italy. E-mail: valerio.carelli@unibo.it

From the [1]IRCCS Institute of Neurological Sciences of Bologna, Bellaria Hospital, Bologna, Italy; [2]Unit of Neurology, Department of Biomedical and Neuromotor Sciences, University of Bologna, Bologna, Italy; [3]Department of Neuroscience, University of Messina, Messina, Italy; [4]Department of Pharmacy and Biotechnology, University of Bologna, Bologna, Italy; [5]Studio Oculistico D'Azeglio, Bologna, Italy; [6]Ophthalmology Clinic, University of Messina, Messina, Italy; [7]Mendel Laboratory, IRCCS Casa Sollievo della Sofferenza, San Giovanni Rotondo, Foggia, Italy; [8]Department of Morphology, Surgery, and Experimental Medicine, University of Ferrara, Ferrara, Italy; [9]Functional Magnetic Resonance Unit, St Orsola-Malpighi Polyclinic, Department of Biomedical and Neuromotor Sciences, University of Bologna, Bologna, Italy; and [10]Mitochondrial Biology Unit, Medical Research Council, Cambridge, United Kingdom

Additional Supporting Information may be found in the online version of this article.

Interpretation: The association of CPEO and parkinsonism/dementia with subclinical optic neuropathy widens the phenotypic spectrum of *OPA1* mutations, highlighting the association of defective mitochondrial dynamics, mtDNA multiple deletions, and altered mitophagy with parkinsonism.

ANN NEUROL 2015;78:21–38

The pathologic accumulation of multiple deletions of mtDNA in skeletal muscle is a hallmark of a relatively homogeneous group of mitochondrial disorders characterized by chronic progressive external ophthalmoplegia (CPEO) and mitochondrial myopathy, inherited as an autosomal dominant or recessive trait.[1,2] Most of these cases are caused by mutations in nuclear genes directly involved in mtDNA replication and maintenance, that is, *POLG*[3] and *POLG2*,[4] encoding the 2 subunits of mtDNA polymerase, *C10orf2*,[5] encoding the mtDNA helicase Twinkle, and *DNA2*,[6] encoding an mtDNA helicase/nuclease. Mutations in genes that control the mitochondrial nucleotide pools can also be associated with this phenotype, including *SLC25A4*,[7] encoding the heart/muscle-specific adenine nucleotide translocator ANT1, *TYMP*,[8] encoding thymidine phosphorylase, *TK2*,[9] encoding the mitochondrial thymidine kinase, *RRM2B*,[10] encoding the p53-sensitive subunit of ribonucleoside reductase, and *DGUOK*,[11] encoding mitochondrial deoxyguanosine kinase. A further gene associated with mtDNA depletion and multiple deletions is *MPV17*,[12] for which the protein function remains unclear. The clinical spectrum varies from a pure myopathy to a complex multisystem condition, with the involvement of both the peripheral and the central nervous systems. Remarkably, L-dopa–responsive parkinsonism has been reported as a prominent late onset clinical feature of several CPEO/myopathy patients associated with *POLG*, *C10orf2*, and *MPV17* mutations.[12–14] In turn, accumulation of multiple mtDNA deletions up to pathological levels has been documented in dopaminergic neurons of the substantia nigra in patients with idiopathic Parkinson disease.[15]

We and others have recently added *OPA1* to the list of genes responsible for accumulation of multiple mtDNA deletions.[16,17] Whereas most of the *OPA1* mutations cause nonsyndromic, dominant optic atrophy (DOA), Kjer type (Online Mendelian Inheritance in Man database #165500; see www.mitodyn.org),[18–20] a set of missense mutations in the guanosine triphosphatase (GTPase) domain, are associated with a DOA-plus syndrome, which can variably include, in addition to optic atrophy, severe sensorineural deafness, cerebellar ataxia, axonal sensorimotor polyneuropathy, and CPEO/mitochondrial myopathy with multiple mtDNA deletions.[16,17,21] In contrast to the previous gene products, which are directly linked to mtDNA replication and nucleotide balance, the OPA1 protein is a dynamin-related GTPase involved in mitochondrial fusion, morphology, and apoptosis.[22] The involvement of specific isoforms of OPA1 in mtDNA maintenance and nucleoid organization has been recently proposed.[23] However, the mechanism linking specific *OPA1* mutations to mtDNA maintenance and instability remains mostly unclear. More recently, a mutation in the *MFN2* gene, also implicated in mitochondrial fusion, was associated with a multisystem disorder characterized by the accumulation of multiple mtDNA deletions.[24]

Here, we report 2 large Italian families comprising 21 patients affected by dominant CPEO/myopathy with multiple mtDNA deletions. Remarkably, 6 of 21 affected members developed parkinsonism and/or dementia. In addition, only 2 subjects had overt visual loss, whereas the others had only mild, late onset optic nerve subatrophy with no visual complaint. Sequence analysis of the *OPA1* gene revealed dominant missense mutations, affecting 2 close amino acid residues in a highly conserved stretch of the OPA1 GTPase domain.

Subjects and Methods

Pedigree Description and Clinical Phenotype

Upon informed consent and approval of the internal review board, we studied 2 families with a dominantly inherited encephalomyopathy, which were originally included in a large survey of patients with *OPA1* mutations.[21] The clinical phenotype was only recently fully characterized, and we report here the details of clinical, genetic, and functional investigations. Family 1 was referred to the IRCCS Institute of Neurological Sciences of Bologna and is composed of 2 apparently unrelated branches, originating from the same geographic area in northern Italy, likely descending from a common founder (Fig 1A). The clinical features of all the affected members are summarized in Supplementary Table 1. Family 2 (see Fig 1B) was referred to the Unit of Neuromuscular Disorders at the University of Messina Medical School. The index case was initially investigated for autosomal dominant CPEO and fatigability. Separately, a second patient suffering of bilateral optic atrophy and parkinsonism was also investigated, and reconstruction of both genealogies revealed that these patients belonged to the same pedigree. Also for this family, the clinical features of the affected individuals are summarized in Supplementary Table 1.

The affected members of both families suffered from a remarkably consistent syndrome including juvenile hypertension and anxiety disorder with panic attacks in the second/third

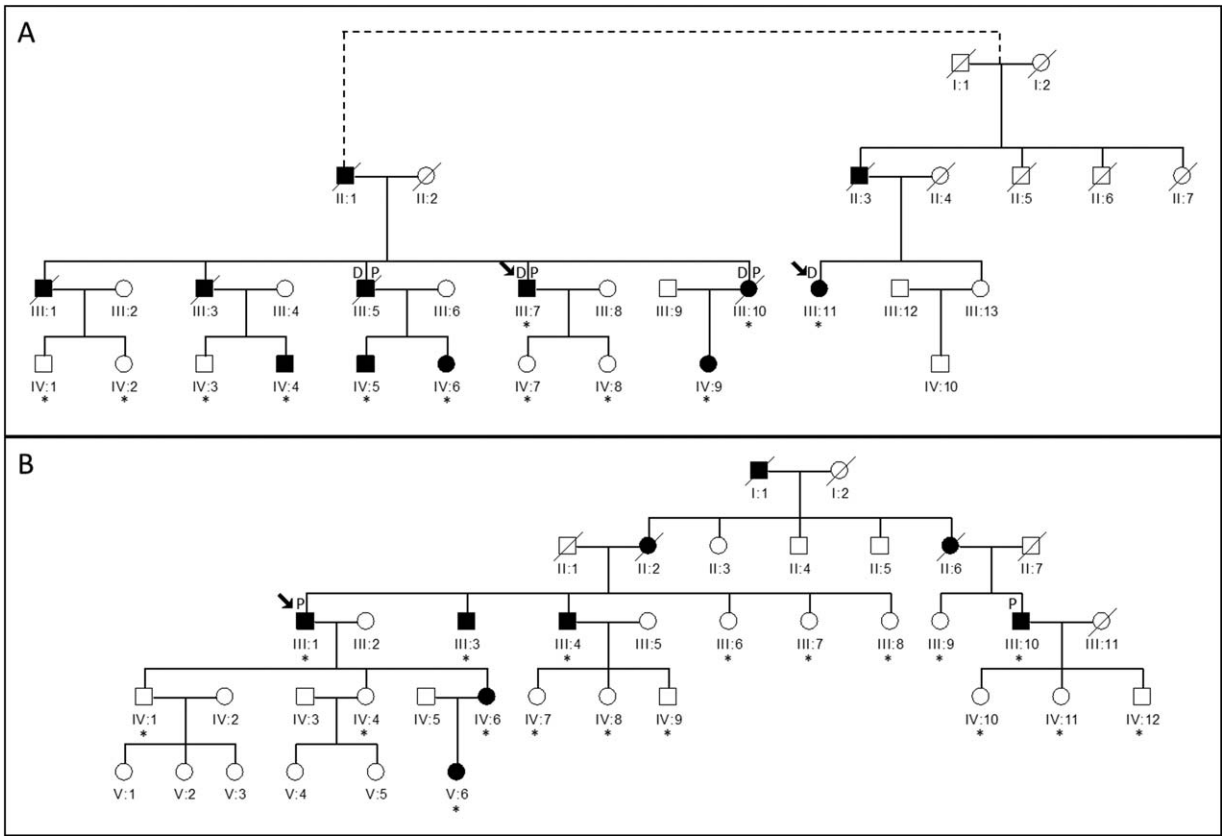

FIGURE 1: Pedigrees of Family 1 (A) and Family 2 (B). The arrows indicate the probands, whereas asterisks indicate family members who underwent genetic analysis. Black symbols denote the affected individuals; the presence of Parkinsonism (P) and dementia (D) are further indicated. Pedigree 1 is composed of 2 branches that share the same founder mutational event, although the parental relationship could not formally be reconstructed.

decade, followed in the third/fourth decade by a combination of slowly progressive ptosis and ophthalmoparesis, mitochondrial myopathy with cytochrome c oxidase (COX)-negative fibers (Fig 2A, B), peripheral neuropathy and cerebellar atrophy leading to mixed ataxia, and sensorineural deafness. Later in life, 6 of these subjects developed parkinsonism (see Supplementary Video of Patient III-7, Family 1) and dementia with diffuse cortical atrophy on brain MRI (Fig 3) and abnormal single photon emission computed tomography (SPECT)/DaT scan (Fig 4). In each family, only a single affected individual had prominent visual loss and optic atrophy, besides the other syndromic features, even if ophthalmological examination could document subclinical optic atrophy in most patients (Fig 5).

Case Reports of the Probands

FAMILY 1 (III:7). This index case is a 72-year-old male who suffered from severe migraine without aura since age 23 years and high blood pressure since age 37 years. At 55 years, he started developing bilateral ptosis, muscle weakness, and gait unsteadiness with occasional falls. He also complained of anxiety and panic attacks. These symptoms progressed over time. At 63 years, he underwent surgery for ptosis on the left eyelid. Our first neurological examination, at age 64 years, revealed right eyelid ptosis, ophthalmoparesis, sensorineural hearing loss, severely reduced vibration sense in the lower limbs, weak/absent deep tendon reflexes, positive Romberg sign, and ataxic gait. Pattern visual evoked potentials (P-VEPs) revealed delayed latency of cortical responses in the left eye, whereas the electroretinogram was normal. Somatosensory evoked potentials (SEPs) revealed delayed central conduction time in the lower limbs. Electroneuromyography disclosed myopathic changes and peripheral axonal sensorimotor polyneuropathy. An audiogram showed bilateral sensorineural selective high-tone hearing loss. He also had hypertension-related cardiomyopathy and first-degree atrioventricular block. Lactic acid after aerobic exercise was slightly increased (29.2mg/dl; normal value [NV] = 5.8–22mg/dl). A muscle biopsy showed myopathic changes with scattered COX-depleted fibers. Idebenone was started (405mg/day) with beneficial effects on the frequency of migraine attacks, improvement of muscle weakness, and normalization of postexercise lactic acid levels. However, the peripheral neuropathy, gait ataxia, and ophthalmoparesis worsened over the years. A neurological evaluation at 68 years revealed postural tremor in the upper limbs. At 69 years, episodes of complex motor behavior during sleep were reported, compatible with rapid eye movement (REM) behavior disorder, and the neurological examination displayed further features including hypomimia, hypophonia, bilateral bradykinesia and rigidity prevalent on the left side, more evident in the upper

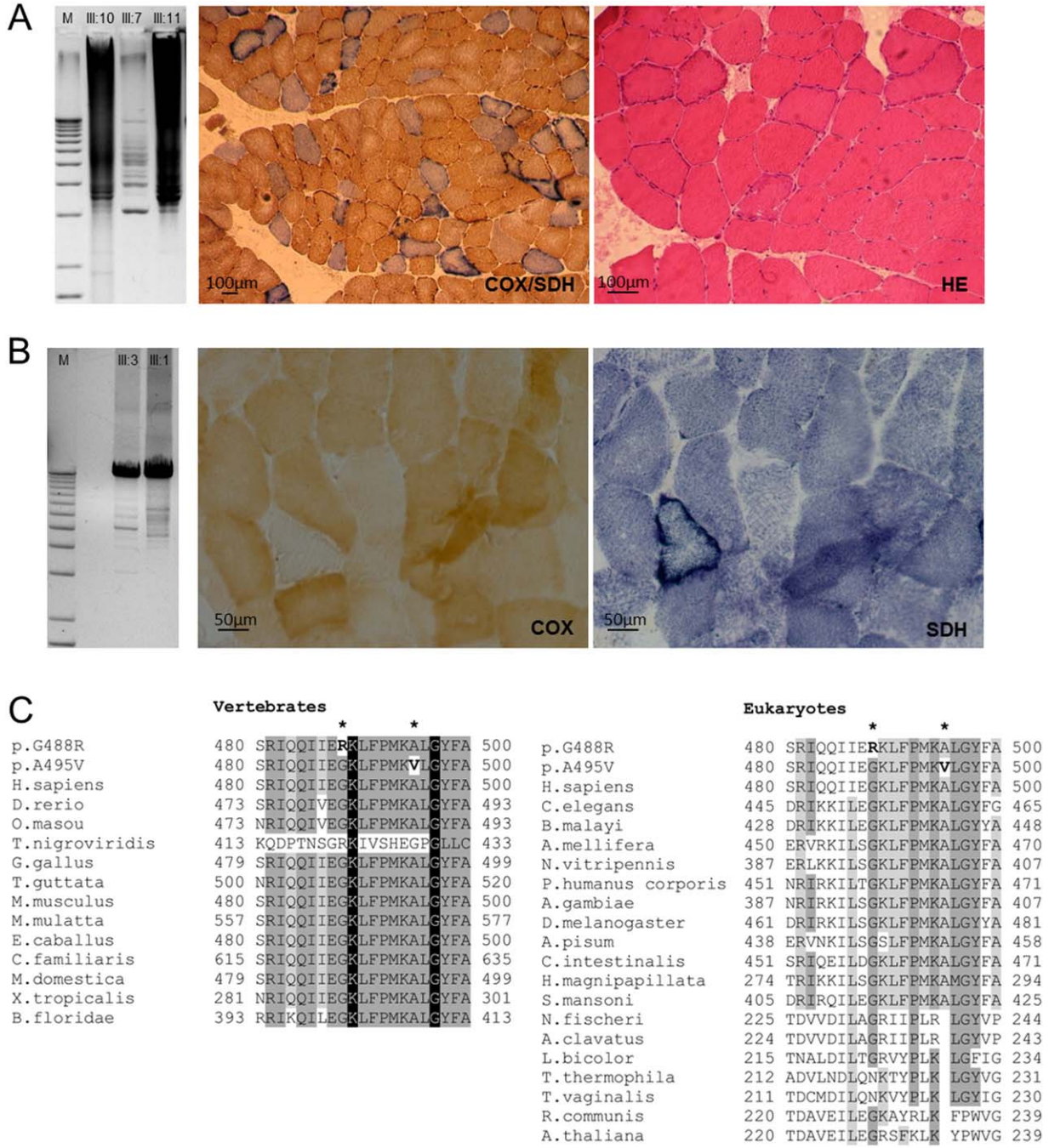

FIGURE 2: mtDNA multiple deletion, muscle histopathology, and OPA1 alignment. (A, B) Long-range polymerase chain reaction shows an accumulation of mtDNA multiple deletions, more abundant in Family 1 (A), and lower in Family 2 (B), congruent with muscle histoenzymatic stainings. Cytochrome c oxidase (COX)/succinate dehydrogenase (SDH) and hematoxylin and eosin (HE) stains show numerous COX-negative and ragged-red fibers in muscle biopsy from Case III:11 (A; Family 1), whereas the muscle biopsy from Case III:1 (B; Family 2) shows only scattered COX-negative fibers and a slight subsarcolemmal increase of SDH reaction. Scale bars = 100μm (A) and 50μm (B). (C) Global alignment of OPA1 protein sequences from eukaryotes shows that both mutations (p.G488R and p.A495R) affect 2 highly conserved residues in vertebrates, contiguous or close to invariant residues. The surrounding protein domain is conserved in eukaryotes and vertebrates. Amino acid residues with a percentage of conservation ranging between 70.0 and 79.9% are highlighted in light gray, those between 80.0 and 99.9% are highlighted in dark gray, and those invariant (100%) are highlighted in black.

limbs, rest and postural tremor in the upper left limb, dystonic posture on the left, slight proximal weakness, and postural instability on pull test (see Supplementary Video). Abnormal autonomic cardiac innervation was evident on myocardial scintigraphy (metaiodobenzylguanidine), and skin biopsy displayed a small-fiber neuropathy. SPECT/DaT scan showed a bilateral presynaptic defect in the putamen (right > left; see Fig 4). Computed tomography (CT) scan revealed basal ganglia

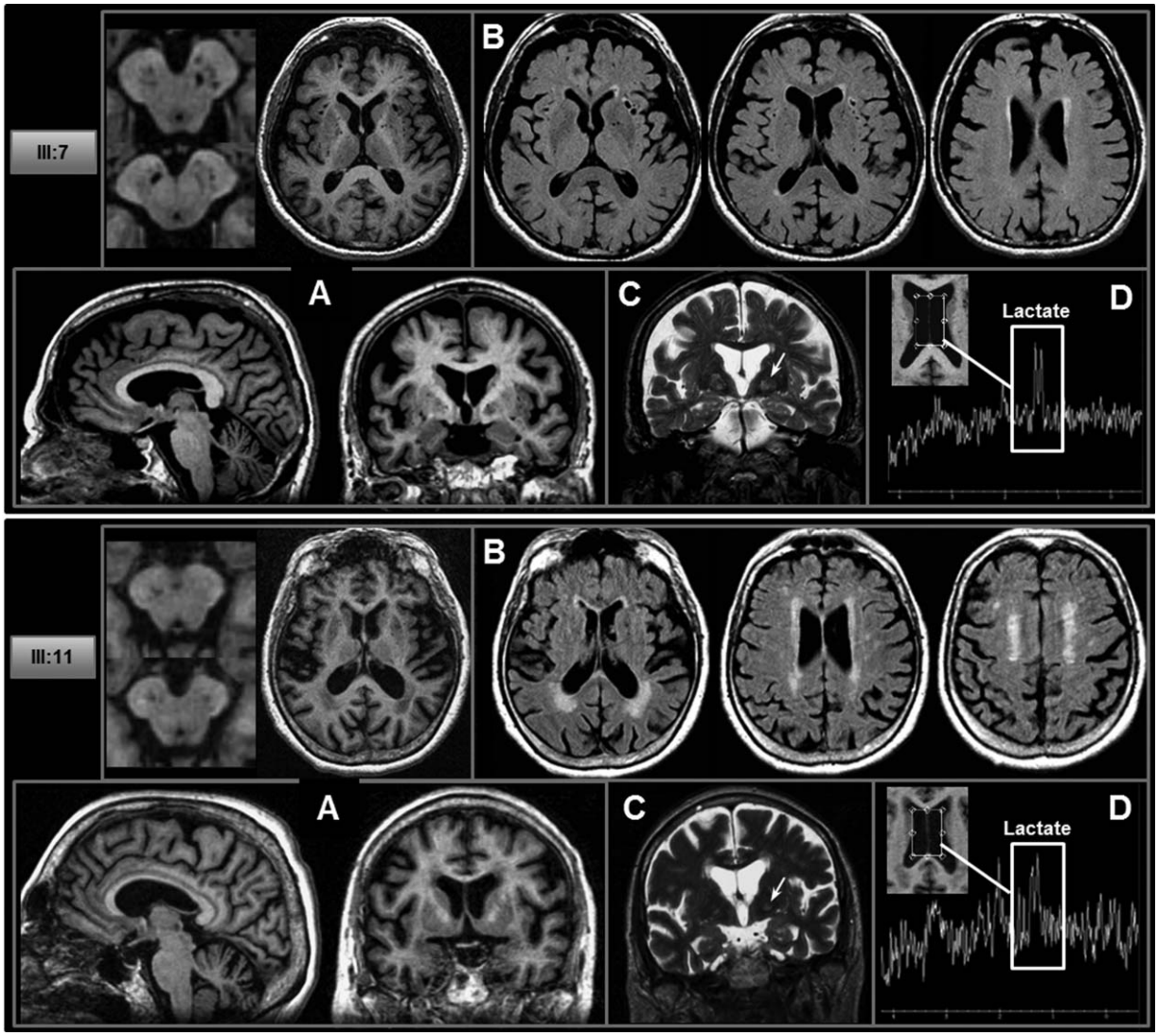

FIGURE 3: Brain magnetic resonance imaging in the 2 probands from Family 1 (III:7 and III:11). (A) Structural 3-dimensional T1 images show cerebral cortical atrophy, mild cerebellar atrophy, and increased perivascular spaces with riddled features at the level of basal ganglia and substantia nigra (see enlarged). (B) Axial fluid-attenuated inversion recovery (FLAIR) T2 images show subcortical lacunar lesions and mild hyperintensity of the periventricular white matter. (C) Coronal fast spin echo T2 images show signal change in the globi pallidi (arrow) that correspond to calcifications on computed tomography scan. (D) Pathological lactate accumulation was detected by proton magnetic resonance spectroscopy at the level of the ventricular cerebrospinal fluid (volume of interest is displayed in the *insert*). Both cases displayed the same lesion pattern with more severe leukoencephalopathy, as evident in the FLAIR T2 images in III:11 (B).

calcifications. Polysomnography showed increased phasic activity during REM sleep, periodic limb movement disorder, and moderate obstructive sleep apnea syndrome. Neuropsychological testing revealed mild multidomain cognitive impairment. Therapy with L-dopa (levodopa/benserazide 200/50.5 × 3/day) and pramipexole (0.36 mg × 2/day) was started with slight improvement of motor symptoms. He continues therapy with idebenone (405 mg/day) and in addition creatine (500 mg/day) and alpha-lipoic acid (600 mg/day).

FAMILY 1 (III:11). This 74-year-old woman started complaining of gait unsteadiness and muscle weakness at 45 years. At age 55 years, she underwent surgery for bilateral eyelid ptosis. Ataxic gait and muscle weakness worsened in the following years. We observed this patient for the first time when she was 67 years old. The neurological examination showed bilateral ptosis and ophthalmoplegia, distal weakness in the upper and lower limbs, intentional tremor, dysdiadochokinesia, distal pain hypoesthesia and loss of vibration sense in the lower limbs, bilateral Babinski sign, absent deep tendon reflexes, positive Romberg sign, and ataxic gait. Blood standard examinations were unremarkable except for slight elevation of creatine kinase (228U/l; NV < 145). Postexercise lactic acid was slightly over the upper limit (23.9mg/dl; NV = 5.8–22mg/dl). Tibial nerve SEPs and motor evoked potentials revealed bilaterally increased central conduction time. Electroneurography showed a moderate axonal sensorimotor polyneuropathy. Audiogram documented mild bilateral sensorineural, high-tone selective hearing loss. Brain CT scan revealed

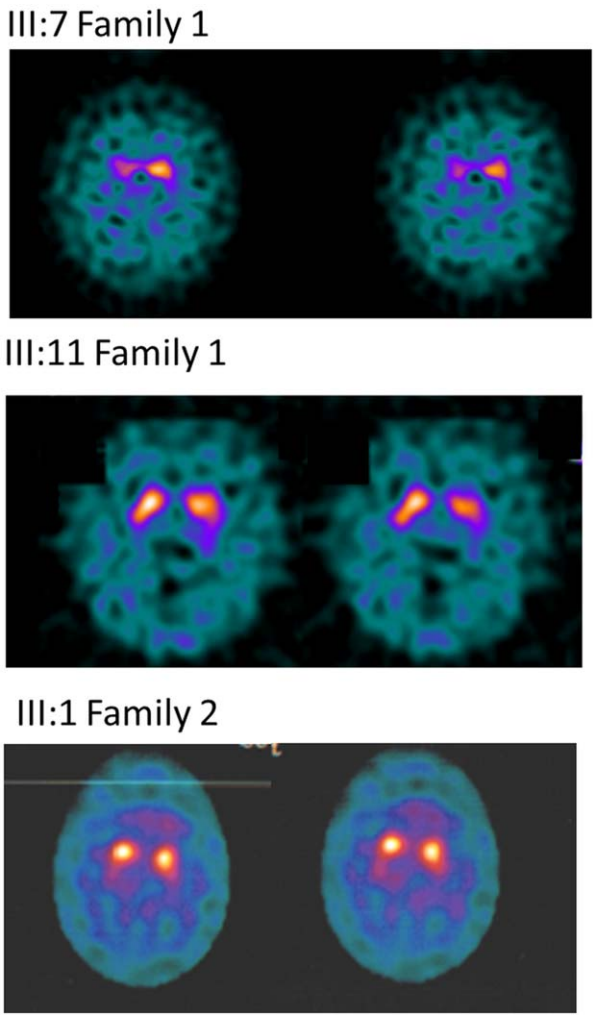

FIGURE 4: Single photon emission computed tomographic imaging/DaT scan in the 3 probands from Family 1 (III-7 and III-11) and Family 2 (III-1). In III-7 (Family 1), with parkinsonism, there is a bilateral dopaminergic defect (right > left). In III-11 (Family 1), with cognitive impairment but without clinical parkinsonism, there is a mild bilateral dopaminergic defect. In III-1 (Family 2), with parkinsonism, there is a bilateral dopaminergic defect (right > left).

bilateral basal ganglia calcifications and diffuse periventricular hypodensities. Muscle biopsy showed marked variability of muscle fibers, and numerous ragged-red fibers (RRF), which were COX-depleted on succinate dehydrogenase (SDH)/COX double stain (see Fig 2A). A mitochondrial disorder was diagnosed, and idebenone therapy was started (up to 675mg/day). The last neurological examination, at 74 years of age, showed cognitive impairment (Mini-Mental State Examination score = 11.7), visual hallucinations, and nocturnal agitation. P-VEPs disclosed the absence of cortical responses. SPECT/DaT scan showed mild bilateral dopaminergic defect (see Fig 4).

FAMILY 2 (III:1). We first observed this patient, now 70 years old, at the age of 55 years. He had bilateral ptosis since he was 50 years old, muscle weakness, and gait unsteadiness, with occasional falls. He had been on therapy for high blood pressure since 37 years of age. He also suffered from anxiety with panic attacks. These symptoms progressed over time. At 60 years of age, he underwent surgery for ptosis on the left eyelid. Neurological examination showed bilateral eyelid ptosis, ophthalmoparesis, deafness, loss of vibration sense in the lower limbs, weak/absent deep tendon reflexes, positive Romberg sign, and mild ataxic gait. Electroneuromyography disclosed myopathic changes and axonal polyneuropathy in the lower limbs. Bilateral sensorineural hearing loss was evident on audiogram. He also had cardiomyopathy and first-degree atrioventricular block requiring pacemaker implantation. Postexercise lactic acid was abnormally elevated (28mg/dl; NV = 5.8–22mg/dl). A muscle biopsy showed myopathy with scattered RRF and COX-depleted fibers (see Fig 2B). At 65 years of age, he presented left upper limb tremor at rest, bradykinesia, and rigidity with frequent falls due to severe unsteadiness. At this time, neurological examination showed hypomimia, bilateral bradykinesia, and plastic hypertonus prevalent on the left side, more evident in the upper limbs, rest and postural tremor of the upper left limb, severe postural instability on pull test, and parkinsonian gait. Cerebral CT scan evidenced bilateral basal ganglia calcifications and diffuse cortical atrophy. SPECT/DaT scan showed a presynaptic defect in both putamina (right > left; see Fig 4). Therapy with L-dopa (levodopa/carbidopa 100/25 1 × 4/day), and pramipexole (0.36mg × 2/day) was started with moderate improvement of motor symptoms.

Ophthalmologic Investigations

Investigated patients had an extensive ophthalmologic examination that included best-corrected visual acuity measurement, slit-lamp biomicroscopy, intraocular pressure measurement, indirect ophthalmoscopy, and visual field testing by Humphrey Field Analyzer (HVF; Humphrey Systems Instruments, Dublin, CA). All subjects also underwent retinal nerve fiber layer (RNFL) and ganglion cell–inner plexiform layer thickness measurements by spectral domain optical coherence tomography (OCT; Cirrus HDOCT, software version 6.0; Carl Zeiss Meditec, Dublin, CA). All scans were acquired using the Optic Disc Cube 200 × 200 and the Macular Cube 512 × 128 protocols as previously described.[25]

MRI and Magnetic Resonance Spectroscopy Evaluation

Brain MRI and brain and skeletal muscle magnetic resonance spectroscopy (MRS) studies were carried out with a 1.5T clinical whole-body magnet (General Electric Medical Systems, Milwaukee, WI). Conventional brain MRI, which included spin-echo T1- and T2-weighted, fluid-attenuated inversion recovery and diffusion-weighted sequences, was performed. For the brain proton MRS (^{1}H-MRS) study, a volume of interest was selected in the lateral ventricles to mostly include the cerebrospinal fluid.[26] The PRESS (Point RESolved Spectroscopy) single voxel localization sequence was used with number of acquisitions = 384, repetition time = 1,500 milliseconds, and echo time = 288 milliseconds chosen to best detect lactate that is normally not detectable in the cerebrospinal fluid. Suppressed water spectra were preprocessed with Gaussian filtering of 2Hz

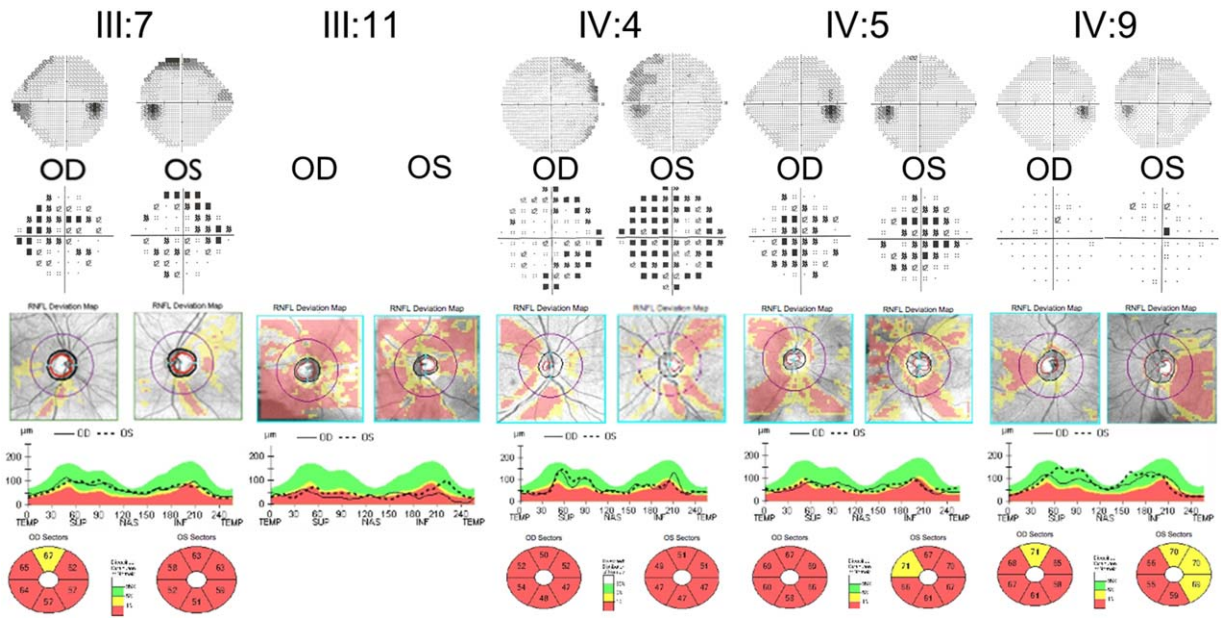

FIGURE 5: Ophthalmological findings in 5 affected subjects from Family 1. (A) Humphrey visual field (total deviation, which indicates the deviation of the patient's results from those of age-matched controls at each test location). (B, C) Spectral domain–optic coherence tomography (SD-OCT) assessments (retinal nerve fiber layer [RNFL]). (D) SD-OCT assessments (ganglion cell–inner plexiform layer [GC-IPL]). Ophthalmological findings show variable degrees of impairment. III-7, the proband, has a subclinical temporal reduction of RNFL thickness, similar to IV-4 and IV-9. Individuals III-11 and IV-5 display a more generalized reduction of RNFL thickness (more severe in III-11). GC-IPL analysis shows a consistent loss of macular retinal ganglion cells in all subjects, IV-9 being the least severe. Correspondingly, visual fields have variable degrees of impairment, mildest in IV:9, whereas III:11 could not complete the examination. OD, oculus destrum; OS, oculus sinistrum; INF, inferior; NAS, nasal; SUP, superior; TEMP, temporal.

followed by exponential filtering of −1Hz, and lactate fitted by the time domain semiparametric algorithm QUEST using jMRUI. The amount of lactate was assessed using unsuppressed water signal as an internal standard.[27]

^{31}P-MRS evaluation of skeletal muscle was performed on the right calf muscle. Spectra were acquired at rest, during an aerobic incremental exercise of plantar flexion, and the following recovery, as previously described.[28] Ten sex- and age-matched healthy controls were also studied. AMARES/MRUI (http://carbon.uab.es/mrui) software analysis was used to quantify phosphorylated compounds. Individual results were taken as abnormal when they fell outside the entire range of the control values.

mtDNA Analysis

Long-range polymerase chain reaction (PCR) on mtDNA was performed to screen for the presence of mtDNA deletions as previously described.[17] Briefly, the set of primers used is as follows: F3485-3519 and R14820-14786 (wild-type mtDNA fragment of 11.335bp), F5459-5493 and R735-701 (wild-type mtDNA fragment of 11.845bp). The PCR conditions were 1 cycle at 94 °C for 1 minute; 30 cycles at 98 °C for 10 seconds, and 68 °C for 11 minutes, followed by a final superextension cycle at 72 °C for 10 minutes. The PCR was performed using Takara Ex Taq DNA polymerase (Takara Shuzo, Kyoto, Japan). The PCR products were separated on a 0.8% agarose gel.

Quantification of mtDNA relative to nuclear DNA (nDNA) was performed by a real time PCR-based method. Briefly, a mtDNA fragment (nt 4625–4714) and a nuclear DNA fragment (FasL gene) were coamplified by multiplex PCR. PCR reaction conditions, primers, and probes were as previously detailed.[17] A standard curve for mtDNA and nDNA was generated using serial known dilutions of a vector (kindly provided by Genemore, Modena, Italy) in which the regions used as template for the 2 amplifications were cloned tail to tail, to have a ratio of 1:1 of the reference molecules. The data presented are means of at least 3 independent measurements.

Screening of Nuclear Genes

Direct sequencing of the complete coding region and the exon/intron boundaries of the candidate genes *POLG,*[3] *POLG2,*[4] *C10orf2* (Twinkle),[5] *SLC25A4* (ANT1),[7] *OPA1,*[17] *PINK1,*[29] and *PARK2*[30] were carried out as previously described. Large gene deletions or duplications in *PARK2* and *PINK1* genes were tested by using the MLPA assay for Parkinson disease (SALSA MLPA Kit P051/P052 Parkinson; MRC-Holland, Amsterdam, the Netherlands). The pathogenic role of *OPA1* mutations was investigated by conservation analysis of amino acid residues after alignment of available sequence from 60 eukaryotic species and by in silico analysis using prediction tools available online (Polyphen 2, SIFT, PROVEAN, and SNPs&GO).

Cells and Culture Conditions

Skin fibroblasts were obtained from 5 healthy donors and 5 affected individuals from the 2 families (III:7, III:11, and IV:9 from Family 1 and III:1 and III:4 from Family 2). Fibroblasts

were grown in Dulbecco modified Eagle medium (DMEM) supplemented with 10% fetal bovine serum, 2mM L-glutamine, and antibiotics. For the experiments, fibroblasts were grown in DMEM or in glucose-free DMEM containing 5mM galactose and 5mM pyruvate (DMEM galactose).[31]

Mitochondrial Morphology

Fibroblasts were seeded onto 36mm-diameter dishes and grown in DMEM or DMEM galactose for 48 hours. Mitochondrial morphology was assessed by staining cells with 10nM Mitotracker Red (Life Technologies, Carlsbad, CA) for 30 minutes at 37 °C. Cellular fluorescence images were acquired with an inverted Nikon (Tokyo, Japan) Eclipse Ti-U epifluorescence microscope equipped with a back-illuminated Photometrics Cascade CCD camera (Roper Scientific, Trenton, NJ). Images were collected using a ×63/1.4 oil objective. Data were acquired and analyzed using Metamorph software (Universal Imaging Corporation, Downingtown, PA).

OPA1 Expression

Total RNA from fibroblasts was extracted with QIAmp RNA blood (Qiagen, Valencia, CA) and reverse transcribed, using the Transcriptor First Strand cDNA Synthesis Kit (Roche Diagnostics, Mannheim, Germany) following the manufacturer's protocol. Expression levels of OPA1 were determined by quantitative real time PCR using SYBR Green I chemistry (Roche Diagnostics) and normalized on *TUBB* levels as the reference gene. Oligonucleotides sequences and PCR conditions are available upon request. cDNA was also sequenced as previously described.[32]

Thirty micrograms of cell lysates in radioimmunoprecipitation assay buffer (50mM Tris–Cl pH 7.6, 150mM NaCl, 1% NP-40, 1% NaDOC, 0.1% sodium dodecyl sulfate [SDS], 5mM ethylenediaminetetraacetic acid [EDTA], 100μl/ml of protease inhibitor cocktail) were separated by 8% SDS–polyacrylamide gel electrophoresis and transferred onto a nitrocellulose membrane (Bio-Rad Laboratories, Hercules, CA). The primary antibodies used were anti-OPA1 (BD Biosciences, Franklin Lakes, NJ; O19820), anti–β-tubulin (Sigma-Aldrich, St Louis, MO; T6557), and anti-VDAC (BioVision, Mountain View, CA; 3594). Detection and densitometry were performed with the Gel Logic 1500 imaging system (Eastman Kodak, Rochester, NY).

Adenosine Triphosphate Synthesis Assay

The mitochondrial adenosine triphosphate (ATP) synthesis was measured in digitonin-permeabilized cells (10×10^6/ml) incubated in 150mM KCl, 25mM Tris-HCl, 2mM EDTA, 0.1% bovine serum albumin, 10mM potassium-phosphate, 0.1mM $MgCl_2$ pH 7.4, in the presence of the inhibitor of adenylate kinase (0.1mM P^1,P^5-di[adenosine-5′] pentaphosphate), by using the luciferin/luciferase assay, as detailed by the manufacturer's instructions. Aliquots of cells (0.1–0.2mg protein) were incubated with 5mM malate plus 5mM pyruvate (complex I substrates), with 10mM succinate plus 2μg/ml rotenone (complex II substrate), or with 25mM glycerol-3-phosphate plus 2μg/ml rotenone (glycerol 3-phosphate dehydrogenase substrate). The reaction was started by addition of 0.1mM adenosine diphosphate (ADP) in the presence of luciferin/luciferase, and chemiluminescence was determined as a function of time with a luminometer (bioORBIT; bioWORLD, Dublin, OH). After addition of 10μM oligomycin, the chemiluminescence signal was calibrated with an internal ATP standard. Data were normalized for citrate synthase activity.[31,33] The ATP monitoring kit, digitonin, P^1,P^5-di(adenosine-5′) pentaphosphate, oligomycin, rotenone, ADP, and all the substrates of the respiratory complexes were from Sigma-Aldrich.

Mitochondrial Membrane Potential

Cells were seeded onto 24mm-diameter round glass cover slips and grown for 2 days in DMEM. Mitochondrial membrane potential ($\Delta\psi_m$) was measured based on the accumulation of tetramethylrhodamine methyl ester (TMRM; Life Technologies) as previously reported.[34] Cells were incubated in bicarbonate-free and phenol red–free Hank balanced salt solution supplemented with 10mM N-2-hydroxyethylpiperazine-N′-2-ethanesulfonic acid and loaded with 20nM TMRM for 30 minutes. At the end of each experiment, mitochondria were fully depolarized by the addition of 4μM of the protonophore carbonyl cyanide 4-(trifluoromethoxy) phenylhydrazone (FCCP; Sigma-Aldrich). Cellular fluorescence images were acquired with an inverted Nikon Eclipse Ti-U epifluorescence microscope equipped with a back-illuminated Photometrics Cascade CCD camera (Roper Scientific). For detection of fluorescence, 568 ± 25nm bandpass excitation and 585nm long pass emission filter settings were used. Images were collected with an exposure time of 100 milliseconds using a ×63/1.4 oil objective. Data were acquired and analyzed using MetaFluor software (Universal Imaging Corporation). Clusters of several mitochondria were identified as regions of interest, and fields not containing cells were taken as background. Sequential digital images and fluorescence intensity were acquired every minute. Fluorescence values were obtained by subtracting background values from those of corresponding mitochondrial areas of interest, for each time point, and expressed as percentage of T0 (100%).

Autophagy Assays

For immunoblotting cells were lysed in a buffer containing 10mM Tris pH 7.4, 150mM NaCl, 1% Triton X-100, 10% glycerol, 10mM EDTA, and protease inhibitor cocktail. After 30 minutes of incubation on ice, the lysates were centrifuged at 12,000 × *g* at 4 °C for 10 minutes. Protein extracts (25μg) were separated on 4 to 20% Tris-Glycine Gel (Life Technologies) and electron-transferred to polyvinylidene difluoride or nitrocellulose membrane according to standard procedures.

The following antibodies were used: anti-LC3B (Sigma-Aldrich, L7543) and anti-ACTB (Sigma-Aldrich, A2668). Other chemicals used are the following: rapamycin (Calbiochem, San Diego, CA; CAS 53123-88-9), FCCP (Sigma-Aldrich, C2920), and ammonium chloride (NH_4Cl; Sigma-Aldrich, A9434).

Fluorescence Microscopy and Quantitative Analysis of Mitophagy

Human skin fibroblast cells were cultured on 24mm glass coverslips in complete medium and treated or not with DMEM

galactose for 48 hours. Before experiments, cells were loaded with LysoTracker Red DND-99 (Life Technologies) to mark lysosomal structures (red) and MitoTracker Green FM (Life Technologies) to visualize mitochondria (green) for 15 minutes. The degree of colocalization of mitochondria with lysosomes was measured via cell live imaging microscopy at 37 °C and 5% CO2 atmosphere using a Nikon Swept Field confocal microscope equipped with CFI Plan Apo VC60XH objective/numerical aperture 1.4, appropriate filter sets (Nikon Instruments), and an Andor DU885 EM-CCD camera (Andor Technology, Belfast, UK); pinhole size was set to allow an optical sectioning of 0.8μm. Confocal images of single planes were acquired and analyzed with identical settings. Statistical evaluation of colocalization was carried out using the colocalization counter JACOP available with Fiji software. The whole area of each live cell with complete mitochondrial and lysosomal staining was margined as a region of interest and applied to colocalization analysis with the threshold setting in channel 1 (red) and channel 2 (green). Finally, object-based colocalization analysis by fluorescence intensity profiles and connexity analysis were used to measure the colocalization of LysoTracker Red and MitoTracker Green fluorescence.

The production of photomicrographs was performed by applying the CROP function of Fiji software to the fluorescent confocal merge images (×4 and ×8 from the original picture, respectively). Because the magnification was relatively high, we improved the quality of the zoomed area performing some graphical adjustments. We first applied a smoothing of the image followed by a correction of the background and, as a final step, a linear correction of brightness and contrast of the merged zoomed areas.

Statistical Analysis

The data were analyzed using Student t test, unless otherwise indicated. Only values of $p < 0.05$ were considered significant.

Results

Ophthalmologic Assessment

We investigated a total of 10 affected individuals, 5 from each family. The details of ophthalmological assessment are summarized in Supplementary Table 2. Overall, only 2 subjects, 1 from each family (IV:4 from Family 1 and III:10 from Family 2, see Supplementary Table 1), had visual complaints that brought them to medical observation. Six of the remaining 8 individuals displayed subclinical optic neuropathy with variable degrees of temporal pallor, decrease of RNFL thickness, loss of macular retinal ganglion cells (RGCs), reduced visual acuity, and defects of the visual field (see Fig 5). None of these patients complained of visual symptoms.

MRI and MRS Evaluation

Two subjects from Family 1 (III:7 and III:11) underwent cerebral MRI, ^{1}H-MRS, and muscle phosphorus-MRS (^{31}P-MRS). Brain MRI showed cerebral cortical atrophy, mild cerebellar atrophy, increased perivascular spaces with riddled features at the level of basal ganglia and substantia nigra, and subcortical white matter signal changes (see Fig 3). Moreover, brain ^{1}H-MRS showed a pathological ventricular accumulation of lactic acid (see Fig 3) and ^{31}P-MRS a significantly delayed resynthesis of phosphocreatine, indicating moderately/severely defective oxidative phosphorylation (OXPHOS; data not shown).

Follow-up ^{1}H-MRS examination performed in Subject III:11 4 years later did not reveal significant changes, whereas the ^{31}P-MRS examination showed severe worsening of the rate of phosphocreatine resynthesis (data not shown).

Genetic Investigations

The mtDNA analysis of available muscle biopsies from Family 1 (III:7, III:10, III:11) showed variable amounts of multiple deletions by long-range PCR, according to the abundance of COX-negative and RRF fibers (see Fig 2A). The same analysis on 2 subjects from Family 2 (III:1, III:3) also showed the presence of some multiple deletions, but these were less abundant compared to Family 1, a finding compatible with the rare occurrence or absence of COX-negative fibers on histoenzymatic staining (see Fig 2B).

Screening of candidates genes (*POLG*, *POLG2*, *C10orf2*-Twinkle, *SLC25A4*-ANT1, and *OPA1*) in the 3 probands (arrows in Fig 1) revealed 2 heterozygous missense mutations in *OPA1*, affecting nucleotide c.1462G>A in Family 1 and c.1484C>T in Family 2. Both these mutations change 2 conserved amino acids close to each other (p.G488R and p.A495V, respectively) in the GTPase domain of OPA1 (see Fig 2C). Prediction tools suggested a pathogenic role for both, and both cosegregated with the pathological phenotype in the families (see Fig 1). We also excluded the occurrence of pathogenic variants or exonic rearrangements in the *PINK1* and *PARK2* genes, as potential genetic modifying factors favoring the occurrence of parkinsonian features in association with the *OPA1* mutations.

Morphological and Biochemical Analysis in Fibroblast Cell Lines

Mitochondrial network morphology was investigated in fibroblasts bearing the p.G488R and the p.A495V *OPA1* mutations, after 48 hours incubation in galactose medium, a well-established condition that forces cells to rely on OXPHOS for ATP synthesis.[35] Whereas control fibroblasts maintained a mitochondrial filamentous network, mutant fibroblasts showed marked mitochondrial fragmentation (Fig 6A). The fibroblasts were scored into

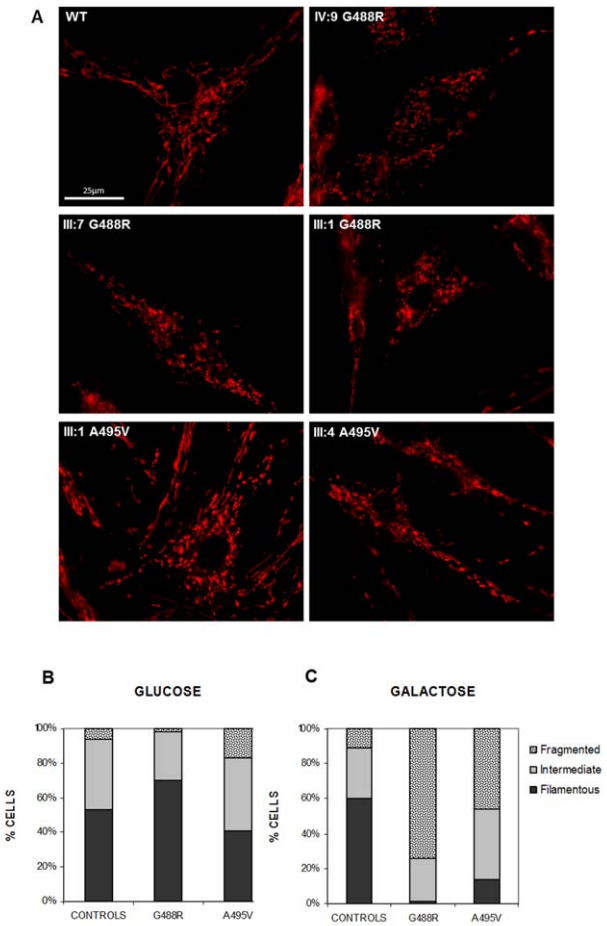

FIGURE 6: Morphology of mitochondrial network. (A) Control (n = 3) and patient (n = 5) fibroblasts were incubated in Dulbecco modified Eagle medium galactose for 48 hours, and then loaded with MitoTracker Red as described in Subjects and Methods. Representatives of eight similar images are shown for each cell line. Scale bar = 25μm. WT = wild type. (B, C) Bar graphs show the distribution of the fibroblasts into 3 different categories on the basis of mitochondrial morphology (filamentous, intermediate, and fragmented) by blind test. Twenty-six control fibroblasts, 21 fibroblasts with the p.G488R mutation, and 34 with the p.A495V mutation were counted in glucose medium; 20 control fibroblasts, 29 fibroblasts with the p.G488R mutation, and 33 with the p.A495V mutation were counted in galactose medium. Fibroblasts analyzed were from 3 control subjects, 3 subjects with the p.G488R mutation, and 2 with the p.A495V mutation.

3 categories based on mitochondrial morphology: cells with filamentous and interconnected mitochondria (filamentous), cells with long mitochondria mixed with short mitochondria (intermediate), and cells with completely fragmented mitochondria (fragmented).

In glucose medium, both control and *OPA1* mutant fibroblasts exhibited a similar percentage of filamentous, intermediate, and fragmented cells (see Fig 6B). After 48 hours of incubation in galactose medium, control fibroblasts maintained the same distribution of the 3 categories, whereas in fibroblasts with the p.G488R mutation the percentage of cells with filamentous mitochondria disappeared and the fragmented mitochondria consistently increased. A similar, albeit less severe, pattern was observed for the fibroblasts with the p.A495V mutation (see Fig 6C). These findings resemble those previously reported in fibroblasts carrying different *OPA1* mutations predicted to cause haploinsufficiency.[31] Interestingly, Western blot analysis revealed a decreased amount of OPA1 protein in fibroblast cell lines from both families, suggesting that these missense mutations were also leading to haploinsufficiency (Fig 7A, B). Quantitative PCR on retrotranscribed OPA1 mRNA in the same fibroblasts from *OPA1* mutant and controls revealed comparable content of OPA1 transcript with similar transcription rates between the mutant and the normal alleles (data not shown), thus excluding the occurrence of RNA decay as the cause of decreased protein amount.

To investigate the bioenergetic competence of *OPA1* mutant fibroblasts, we measured the rate of ATP synthesis in digitonin-permeabilized cells, after normalization for citrate synthase activity, a widely used indicator of mitochondrial mass.[33] As reported in Figure 7C, the rate of ATP synthesis driven by complex I substrates (pyruvate and malate) was significantly decreased in fibroblasts with the p.G488R *OPA1* mutations compared to controls, whereas the fibroblasts with the p.A495V *OPA1* mutation showed no reduction. ATP synthesis driven by substrates feeding complex II (succinate) or mitochondrial glycerol 3-phosphate dehydrogenase (glycerol 3-phosphate) failed to show significant differences, although a tendency toward reduction for complex II–driven ATP synthesis was present in patients' fibroblasts (see Fig 7C).

We next evaluated $\Delta\psi_m$ as assessed by the mitochondrial loading of TMRM, a fluorescent cationic probe that accumulates in polarized mitochondria and is released when $\Delta\psi_m$ decreases. In control fibroblasts $\Delta\psi_m$ was maintained in the presence of the ATP-synthase inhibitor oligomycin, whereas it was slightly but significantly decreased in fibroblasts with the p.A495V mutation. In contrast, oligomycin induced a rapid and significant decrease of $\Delta\psi_m$ in fibroblasts with the p.G488R mutation (see Fig 7D). Noticeably, there were no differences at baseline $\Delta\psi_m$ between OPA1 mutants and control fibroblasts. These results indicate that p.A495V mutant fibroblasts, more severely than those carrying the pG488R mutation, were both unable to maintain the membrane potential exclusively through the respiratory chain and had to exploit ATPase-mediated ATP hydrolysis to generate $\Delta\psi_m$.

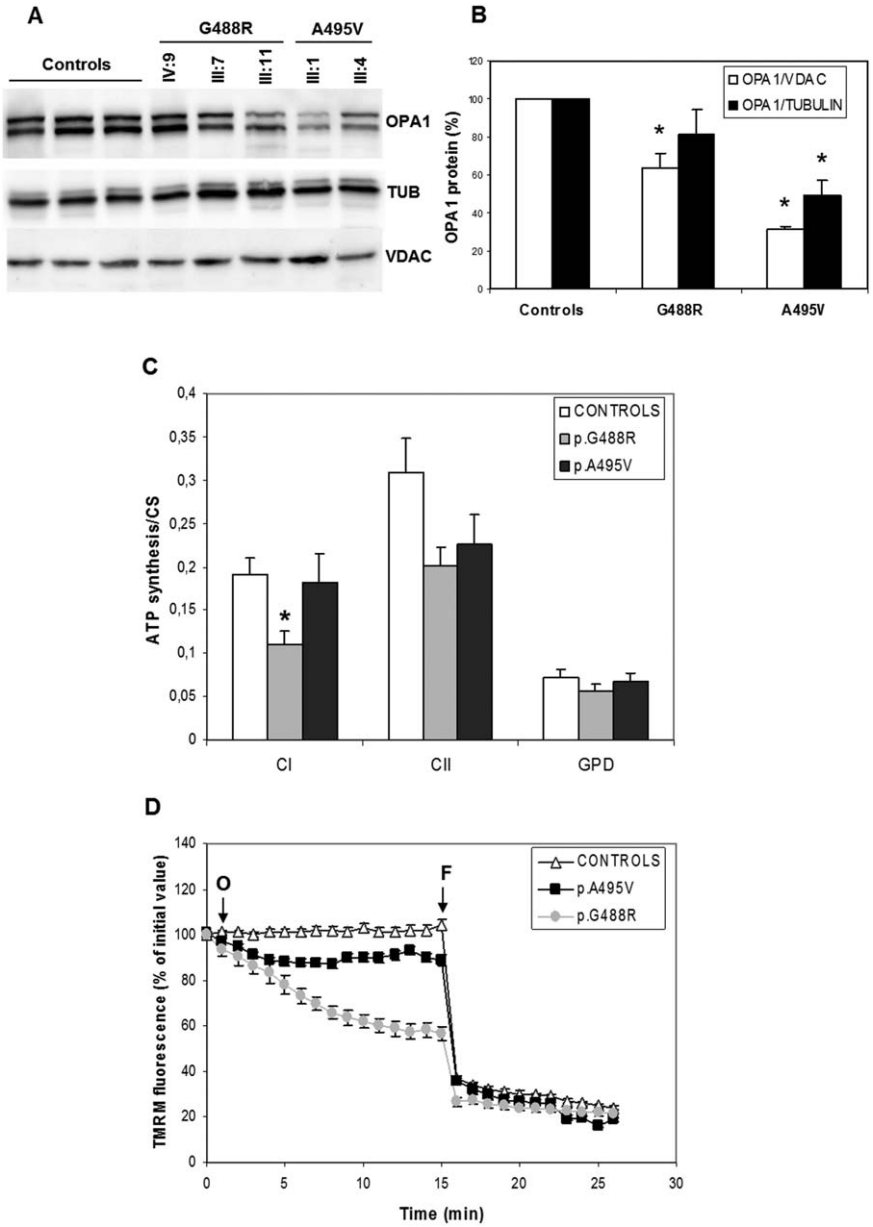

FIGURE 7: OPA1 protein amount and bioenergetics in control and mutant fibroblasts. (A) Representative Western blot of OPA1, b-tubulin, and VDAC was carried out in fibroblast lysates obtained from 3 controls and from patients carrying the indicated *OPA1* mutations. (B) OPA1 bands were normalized to β-tubulin and VDAC band density. Results are means ± standard error of the mean (SEM) of 4 controls and the 5 OPA1 mutant fibroblast lysates obtained from 3 independent experiments and resolved in at least 3 blots. Asterisks denote values significantly different from controls ($p < 0.05$). (C) Mitochondrial adenosine triphosphate (ATP) synthesis. Fibroblasts were treated with 50μg/ml digitonin, and the rate of ATP synthesis driven by 5mM pyruvate plus 5mM malate (complex I), 10mM succinate plus 4mM rotenone (complex II), or 25mM glycerol 3-phosphate plus 4mM rotenone (mitochondrial glycerol phosphate dehydrogenase) was subsequently determined. The rate of ATP synthesis was normalized for citrate synthase (CS) activity. Data (mean ± SEM) were obtained from 5 controls and the 5 OPA1 mutant fibroblasts grouped by mutation type. The experiment was performed at least in triplicate. Asterisk denotes values significantly different from controls ($p < 0.05$). (D) Effect of oligomycin on mitochondrial membrane potential. Control and OPA1 mutant fibroblasts were loaded with tetramethylrhodamine methyl ester (TMRM) as described Subjects and Methods. Where indicated, 6μM oligomycin (O) and 4μM carbonyl cyanide 4-(trifluoromethoxy) phenylhydrazone (FCCP; F) were added. Data are mean ± SEM ($n = 10$). Fluorescence readings following the addition of oligomycin and preceding that of FCCP revealed a statistically significant difference ($p < 0.05$) for all time points between fibroblasts with the p.G488R mutation and both controls and fibroblasts with the p.A495V mutation.

Autophagy and Mitophagy Assessment in Fibroblasts

To evaluate whether alterations of the autophagic machinery affected *OPA1* mutant fibroblasts compared to controls, we quantified the levels of autophagy. Microtubule-associated protein 1 light chain 3 (MAP1LC3, hereafter referred to as LC3), a mammalian homolog of yeast Atg8, is used as a specific marker to monitor autophagy.[36] During autophagy, the cytoplasmic form (LC3-I) is processed to a cleaved and lipidated membrane-bound form (LC3-II), which is localized to the autophagosome. This conversion can be measured by immunoblotting with antibodies against LC3, which usually reveals 2 bands: LC3-I (16kDa) and LC3-II (14kDa). The amount of LC3-II correlates well with the number of autophagosomes.[37]

We compared the levels of autophagy in resting conditions (DMEM), after incubation in galactose medium (DMEM galactose), and after exposure to a strong autophagic inducer such as rapamycin, an mTOR inhibitor (Fig 8A, B). We found that in basal conditions *OPA1* mutant fibroblasts displayed higher amounts of the endogenous LC3-II levels compared to control fibroblasts, as revealed by immunoblot analysis of LC3-II levels, suggesting increased autophagy in the *OPA1* mutant patients. Shifting cells from glucose to galactose medium greatly activated autophagy in both controls and OPA1 mutant fibroblasts (see Fig 8A). This activation was also exerted by rapamycin, but was less evident for OPA1 mutant cells, which already had high autophagic activity (see Fig 8B).

A common misconception is that increased number of autophagosomes invariably corresponds to increased cellular autophagic activity. Autophagosome accumulation, and thus increase in the levels of autophagosomal marker LC3, may represent either autophagy induction or impaired degradation of autophagosomes. Consequently, in both conditions, the number of autophagosomes is increased. To distinguish between these 2 scenarios, we performed autophagic flux analysis in control and *OPA1* mutant fibroblasts, evaluating the induction of autophagy in the presence of the lysosomal activity inhibitor NH_4Cl. We found that treatment with NH_4Cl 20μM for 2 hours induces abundant accumulation of the cleaved form of LC3, when compared to untreated conditions. Noticeably, this occurs equally in control and *OPA1* mutant fibroblasts (see Fig 8C), indicating that the autophagic response is unaffected in our experimental conditions. Taken together, these results demonstrate that the autophagic machinery is intrinsically activated in *OPA1* mutant fibroblasts compared to control fibroblasts.

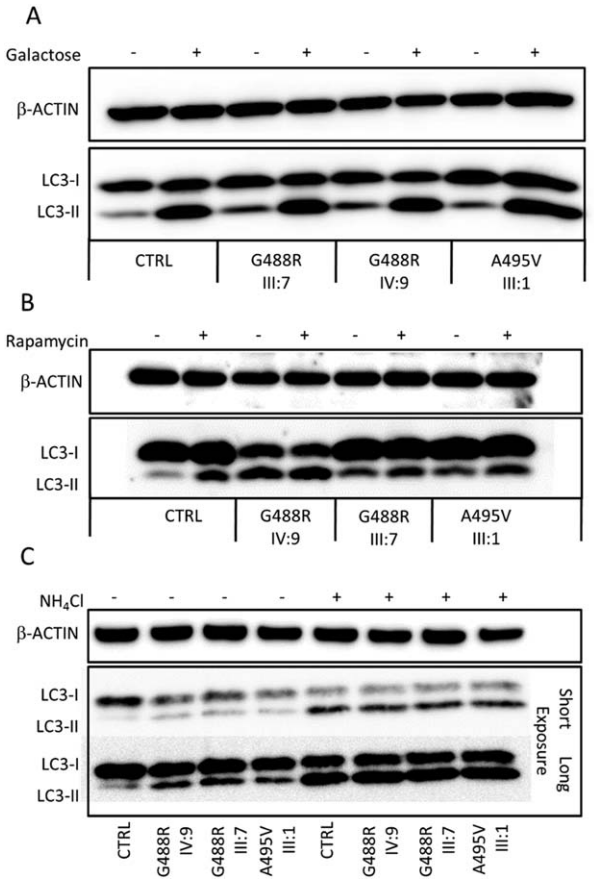

FIGURE 8: Autophagy in control and mutant fibroblasts. Representative immunoblots are shown, documenting the conversion of nonlipidated microtubule-associated protein 1 light chain 3 (LC3)-I to its cleaved and lipidated variant LC3-II in skin fibroblasts obtained from a healthy donor and 3 patients. Where indicated (+), the cells were incubated in Dulbecco modified Eagle medium–galactose for 48 hours (A), rapamycin 10μM for 2 hours (B), and NH_4Cl 20μM for 2 hours (C). As control for the equal loading of lanes, an anti–β-actin antibody was used.

To specifically assess mitophagy, a process deputed to the clearance of damaged mitochondria, we also investigated whether enhanced sequestration of mitochondria was present in autophagic vacuoles of mutant cells. Thus, we performed direct live fluorescence microscopy in fibroblasts loaded with LysoTracker Red (visualizing lysosomal structures) and MitoTracker Green (visualizing mitochondria) to monitor the delivery of mitochondria into the autophagosome (Figs 9A and 10A).[37,38]

As shown in Figure 9, in resting condition, the rate of colocalization between the signal for lysosomes (red) and the signal for mitochondria (green) was higher in all *OPA1* mutant fibroblasts compared to controls, indicating increased mitophagy (see Fig 9B). Galactose induced a significant increase of colocalization only in control fibroblasts, suggesting that in *OPA1* mutant patients the mitophagy rate was already maximal (see Fig 9B).

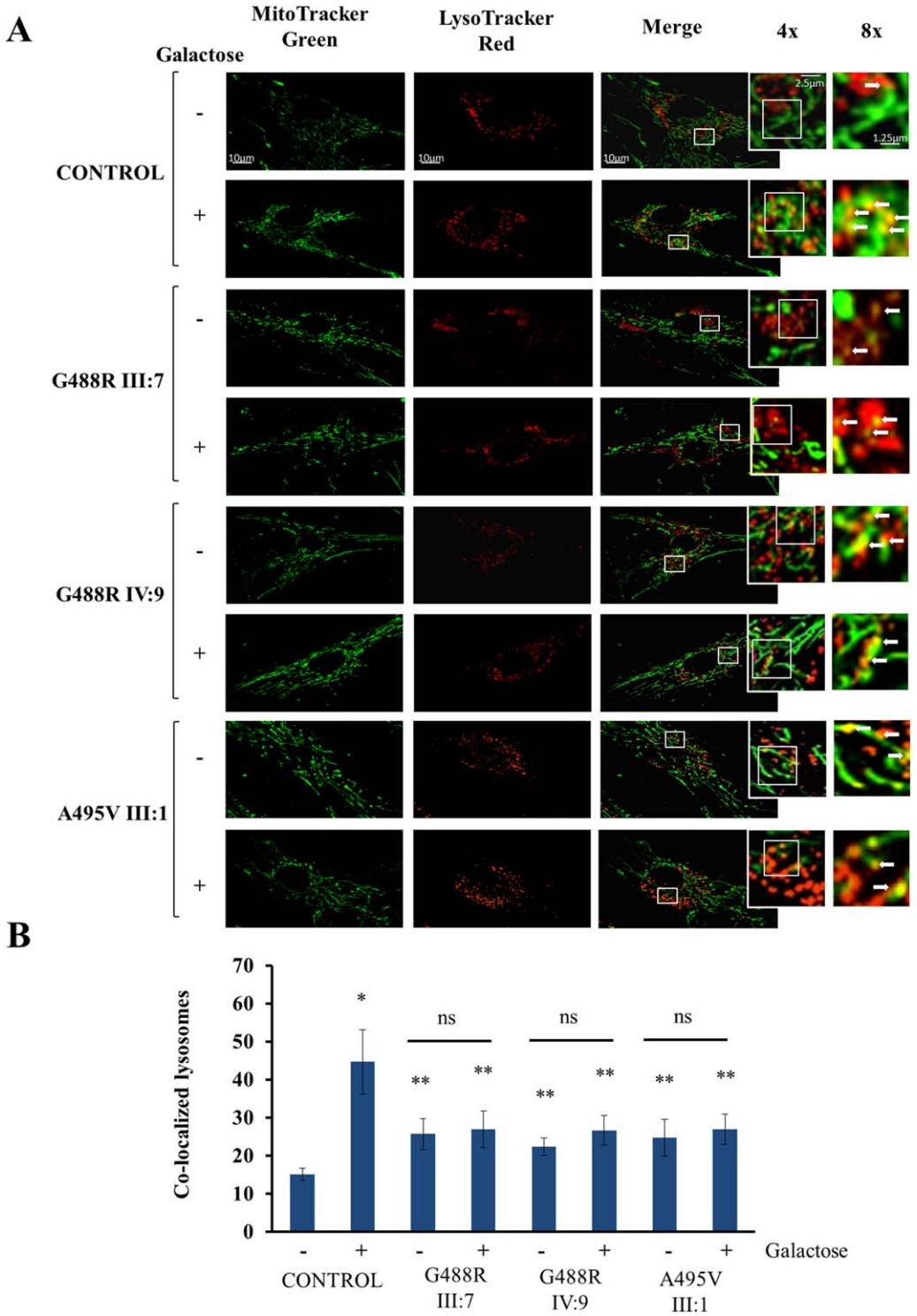

FIGURE 9: Confocal microscopy analysis of mitophagy in control and mutant fibroblasts cultured in glucose and galactose medium. (A) Skin fibroblasts obtained from a healthy donor and 3 investigated patients were incubated in Dulbecco modified Eagle medium (DMEM) glucose or DMEM galactose for 48 hours. Before experiments, cells were loaded with LysoTracker Red and MitoTracker Green to visualize lysosomes and mitochondria, respectively. The degree of the signal of lysosomes with mitochondria (merge) was calculated via cell live imaging microscopy by using a Nikon Swept Field confocal microscope equipped with a CFI Plan Apo VC60XH objective (numerical aperture = 1.4; for details see Subjects and Methods). The confocal images shown are representative of a minimum of 18 cells from at least 3 independent experiments performed in duplicate. Sequentially zoomed regions *(insets)* from the fluorescent confocal merge images (×4 and ×8 from the original picture, respectively) illustrate the lysosome (red signal) and mitochondria (green signal) colocalization, appearing as yellow areas indicative of mitophagy *(arrows)*. Scale bars = 10μm in merge pictures, 2.5μm in ×4 pictures, 1.25μm in ×8 pictures. (B) The graph represents the amount of colocalization between lysosomes (red signal) and mitochondria (green signal). The rate of colocalization of green and red signals was evaluated using the colocalization counter JACOP available in Fiji software. Data are presented as mean ± standard deviation. *$p < 0.01$, **$p < 0.05$; ns = not significant.

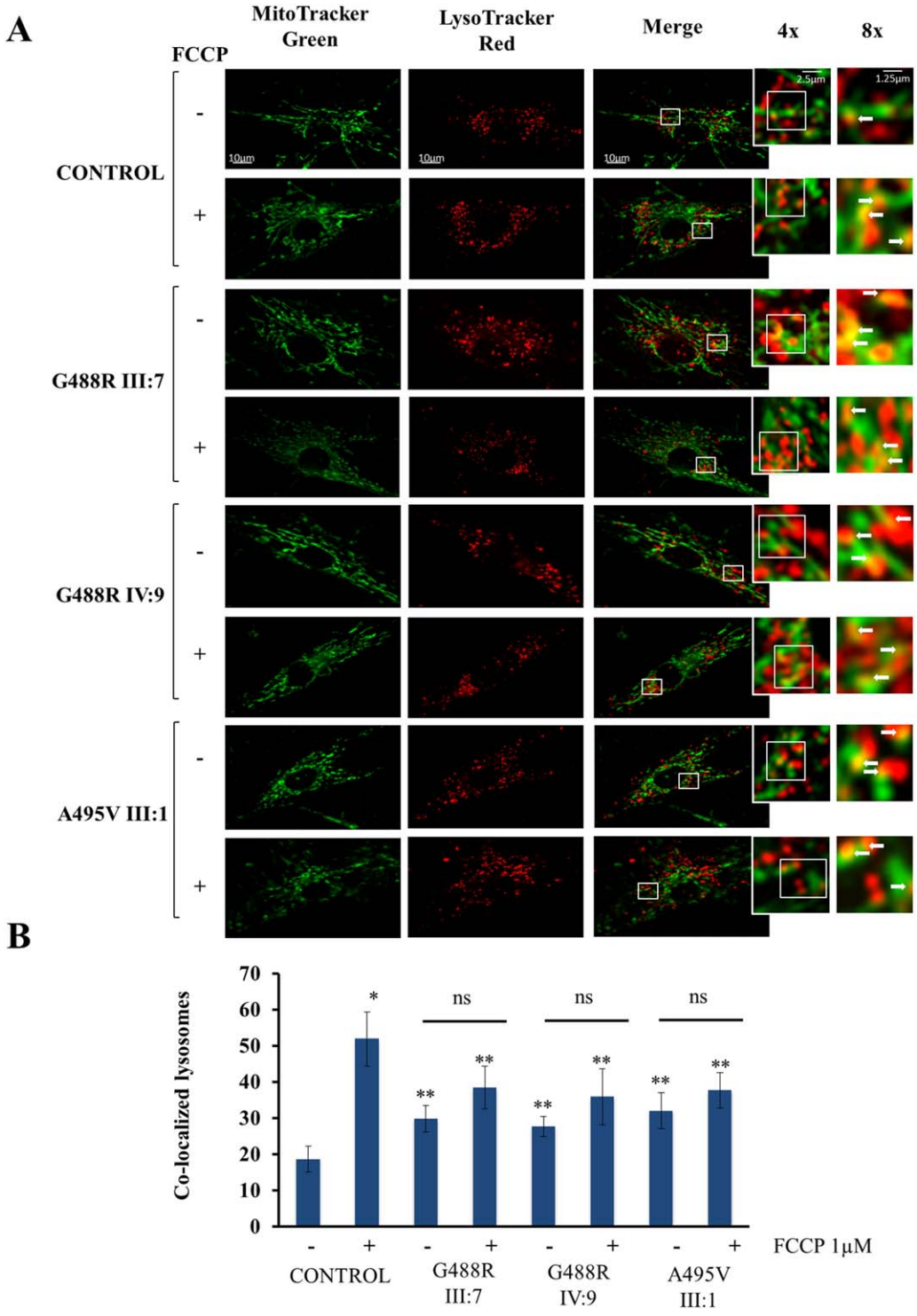

FIGURE 10: Confocal microscopy assessment of mitophagy in control and mutant fibroblasts cultured in glucose and after carbonyl cyanide 4-(trifluoromethoxy) phenylhydrazone (FCCP)-driven uncoupling. (A) Control and mutant fibroblasts were cultured in complete medium and treated with FCCP 1 μM for 30 minutes, under the same colocalization conditions of MitoTracker Green and LysoTracker Red fluorescence as for assessment of mitophagic activity by cell live imaging microscopy. Confocal images were obtained with a Nikon Swept Field confocal microscope equipped with a VC60XH immersion objective lens (numerical aperture = 1.4; for details see Subjects and Methods). The images shown are representative of a minimum of 20 cells from at least 3 independent experiments performed in duplicate. Sequentially zoomed regions *(insets)* from fluorescent confocal merge images (×4 and ×8 from the original picture, respectively) illustrate the lysosome (red signal) and mitochondria (green signal) colocalization, appearing as yellow areas indicative of mitophagy *(arrows)*. Scale bars = 10μm in merge pictures, 2.5μm in ×4 pictures, 1.25μm in ×8 pictures. (B) The graph represents the amount of colocalization between lysosomes (red signal) and mitochondria (green signal). Data are presented as mean ± standard deviation. *$p < 0.01$, **$p < 0.05$; ns = not significant.

To further confirm this result, we pretreated control and *OPA1* mutant fibroblasts with FCCP, a well-known trigger of mitophagy (see Fig 10). After 30 minutes of incubation with 1μM FCCP, the *OPA1* mutant fibroblasts displayed only a slight, nonsignificant increase in the amount of colocalization between red and green signals compared with untreated control fibroblasts (see Fig 10B). In contrast, control fibroblasts under the same treatment significantly raised the number of mitochondria sequestered by lysosomes (see Fig 10B). Overall, these data confirm the initial observation that *OPA1* mutant fibroblasts present higher basal levels of mitophagy compared to control, which could not be fully increased after both galactose and FCCP treatments.

Discussion

This study reports for the first time 2 families with dominant syndromic CPEO complicated by severe neurodegeneration with dementia and parkinsonism, cosegregating with 2 different missense heterozygous mutations affecting close, highly conserved amino acid residues in the GTPase domain of the *OPA1* gene. Both mutations were predicted to be deleterious by multiple approaches. Remarkably, the clinical phenotype was not characterized by a prominent optic neuropathy, the hallmark feature of *OPA1* mutations. Muscle biopsies showed variable degrees of COX-negative fibers with accumulation of mtDNA multiple deletions, as previously seen in DOA-plus cases. In vivo and in vitro functional studies documented impaired OXPHOS, mainly due to complex I deficiency, low membrane potential and abnormal mitochondrial dynamics, associated with decreased content of OPA1 protein, and increased levels of autophagy and mitophagy.

On clinical grounds, 2 features are remarkable. First, loss of vision due to optic atrophy was not the main complaint in the affected individuals, with the exception of 2 cases, 1 in each family, for whom visual loss led to medical consultation and a diagnosis of optic atrophy. These cases were instrumental in directing the genetic investigation to the successful identification of *OPA1* mutations. However, careful neuro-ophthalmological assessment of the affected family members documented, mainly by OCT, the subclinical loss of axons in the papillomacular bundle, as typically seen in DOA. Only 1 *OPA1* mutant patient has been previously reported with CPEO, myalgia, deafness, depression, and mtDNA multiple deletions in muscle, without evidence of optic atrophy.[39] This patient carried a mutation in the mitochondrial targeting sequence of the *OPA1* gene, potentially affecting the protein import within mitochondria.[39]

Second, besides CPEO, myopathy, and peripheral neuropathy, clinical features previously reported in DOA-plus cases, these 2 families were remarkable for the presence of cognitive impairment and/or parkinsonism in many individuals. The occurrence of parkinsonism associates our families with previously reported CPEO syndromes with parkinsonism and mtDNA multiple deletions due to *POLG*, *C10orf2*, and more recently *MPV17* mutations.[12–14] Furthermore, pathologic accumulation of mtDNA multiple deletions in dopaminergic neurons also characterizes idiopathic Parkinson disease, as shown by laser capturing experiments and mtDNA genetic analysis of single neurons from postmortem substantia nigra.[15] In our families, parkinsonism was associated with cognitive impairment and, interestingly, Individual III:11, who had dementia without clinical parkinsonism, also had abnormal dopaminergic uptake in the basal ganglia on SPECT/DaT scan (see Fig 4). Brain imaging showed cerebral cortical atrophy and multiple lesions in basal ganglia and substantia nigra, which are compatible with both cognitive impairment and parkinsonian features of these patients. A consistent recurrence of bilateral calcium deposition in the globi pallidi was also evident in several subjects from both families, a frequent finding in mitochondrial encephalomyopathies, including DOA-plus.[17,21]

Other peculiar clinical features in both families were the occurrence of early onset hypertension and psychiatric disturbances such as panic attacks. These features are neither common nor specific to mitochondrial diseases, but they may both have been overlooked to date, because they are frequent in the general population and difficult to relate to mitochondrial dysfunction.[40–43] However, the striking similarity of both probands from each family (III:7 in Family 1 and III:1 in Family 2) and further recurrence of these features in other individuals suggest that both hypertension and anxiety disorder may be underestimated features in mitochondrial diseases. Previous reports noted depression and anxiety or other psychiatric disturbances in syndromes associated with mtDNA multiple deletions.[40,42]

Functional studies remarked a bioenergetic defect in vivo by ^{1}H-MRS and ^{31}P-MRS. The first analysis demonstrated pathological levels of lactate in brain and cerebrospinal fluid, the second showed impaired skeletal muscle mitochondrial ATP synthesis rate. In vitro analysis in fibroblasts confirmed impaired OXPHOS proficiency. Fibroblasts carrying the p.G488R *OPA1* mutation (Family 1) showed significantly reduced complex I–dependent ATP synthesis and were unable to maintain mitochondrial inner membrane potential after oligomycin inhibition of ATP synthase. Notably, the biochemical

impact of the p.A495V mutation (Family 2) was milder, as ATP synthesis was normal and the membrane potential was only slightly reduced after oligomycin inhibition. This milder biochemical phenotype was likely a consequence of a lower amount of mtDNA multiple deletions detected in the skeletal muscle biopsy and the occurrence of only a few COX-negative fibers compared to individuals from Family 1.

We also demonstrated dysfunctional mitochondrial dynamics, as expected for *OPA1* mutations, with highly fragmented mitochondrial network when fibroblasts were grown in galactose medium. We and others have previously shown this feature in fibroblasts carrying *OPA1* mutations leading to haploinsufficiency linked to nonsyndromic DOA.[31,44] Western blot analysis revealed the somewhat surprising observation that, as also reported for DOA-associated nonsense mutations, both these *OPA1* missense mutations led to decreased OPA1 protein amount, suggesting haploinsufficiency. This was not due to RNA decay, as evidenced by unaffected transcription rates with normal total *OPA1* mRNA content in *OPA1* mutant fibroblasts compared to controls. Thus, we hypothesize that these 2 missense *OPA1* mutations may lead to protein instability and faster OPA1 turnover, but further investigations are clearly needed to resolve this issue.

Finally, we investigated how these 2 *OPA1* mutations may impinge on mitochondrial quality control by assessing autophagic and mitophagic activities. Both basal autophagy and mitophagy in glucose medium were increased in *OPA1* mutant fibroblasts compared with controls, whereas the autophagic flux was normal. We observed that control fibroblasts grown in galactose medium and after uncoupling with FCCP greatly activated autophagy and mitophagy, to a similar extent as with the classic autophagy activator rapamycin. Growing *OPA1* mutant fibroblasts in galactose medium led to further activation of autophagy, but did not increase mitophagy compared to cells grown in glucose, suggesting that *OPA1* mutations activated basal mitophagy to a maximal level that could not be further increased. Under the same experimental conditions, the uncoupler FCCP induced only a slight, nonsignificant increase of mitophagy in *OPA1* mutant fibroblasts, in clear contrast with the levels reached by control fibroblasts in the same conditions. The failure to further activate mitophagy after different stimuli has, to our knowledge, not been previously reported, and we hypothesize that it might be related to the mitochondrial bioenergetic defect observed in the *OPA1* mutant fibroblasts. In particular, impairment of OXPHOS, loss of mitochondrial membrane potential, and mitochondrial network fragmentation are typical features associated with mitophagic removal of mitochondria. Typically, uncoupling agents (FCCP or carbonyl cyanide *m*-chlorophenyl hydrazone, CCCP) promote mitochondrial permeabilization, leading to mitochondrial fragmentation and ultimately sequestration of damaged mitochondria by autophagosomes.[45] It has been shown that mitochondria carrying deleterious mtDNA mutations can be selectively eliminated through mitophagy, and increased autophagy has recently been documented in RGCs in murine models of DOA.[46–48]

Impaired mitophagy has been shown to be a key pathogenic mechanism in autosomal recessive Parkinson disease due to mutations in the *PARK2* (encoding Parkin) and *PINK1* genes, both encoding proteins involved in the quality control of mitochondria and indirectly affecting mitochondrial dynamics and biogenesis.[49,50] Because previous studies have implicated single heterozygous mutations in *PARK2* and *PINK1* as possible risk factors for developing parkinsonism,[51] we performed a comprehensive mutation analysis of both genes in our patients, but failed to identify pathogenic variants. Notably, a direct link was recently established between Parkin and OPA1, through linear ubiquitination of NF-kB essential modulator, which upregulates the expression of OPA1, promoting mitochondrial integrity and protecting from stress-induced cell death.[52] Conversely, alterations in both mitochondrial morphology and ATP production caused by either Parkin or PINK1 loss of function can be rescued by overexpressing the mitochondrial fusion proteins MFN2 and OPA1.[53] Our findings indicate that specific *OPA1* mutations are associated clinically with parkinsonism, thus bridging mitochondrial dynamics, in particular fusion carried out by MFN2 and OPA1, and the quality control gatekeepers Parkin and PINK1. Overall, the common features associating primary mitochondrial diseases and Parkinson disease, such as complex I dysfunction, accumulation of mtDNA multiple deletions, and altered quality control, remain to be fully elucidated.

In conclusion, the 2 families here investigated represent an extreme of a spectrum of *OPA1*-pathies ranging from isolated optic nerve involvement to severe multisystem mitochondrial encephalomyopathy with late onset dementia and parkinsonism. Our functional studies establish the link between primary mitochondrial dysfunction and neurodegeneration, highlighting common pathogenic pathways involving the central theme of mtDNA maintenance and quality control.

Acknowledgment

This study was supported by Telethon–Italy (GGP06233, V.C.; GPP10005, M.Z., V.C.; GGP14187, V.C.),

Programma di ricerca Regione-Università 2010-2012 (PRUa1RI-2012-008, V.C.), and a European Research Council ERC-FP7 advanced grant (322424, M.Z.).

We thank all the patients and their families for participating to this study and Drs M. P. Giannoccaro and M. Fabbri for their help.

Potential Conflicts of Interest

R.Li.: board membership, HPS Health Publishing & Services, Genzyme; travel expenses, Biomarin Europe.

References

1. Zeviani M, Servidei S, Gellera C, et al. An autosomal dominant disorder with multiple deletions of mitochondrial DNA starting at the D-loop region. Nature 1989;339:309–311.
2. Spinazzola A, Zeviani M. Disorders of nuclear-mitochondrial intergenomic communication. Biosci Rep 2007;27:39–51.
3. Van Goethem G, Dermaut B, Lofgren A, et al. Mutation of POLG is associated with progressive external ophthalmoplegia characterized by mtDNA deletions. Nat Genet 2001;28:211–212.
4. Longley MJ, Clark S, Yu Wai Man C, et al. Mutant POLG2 disrupts DNA polymerase gamma subunits and causes progressive external ophthalmoplegia. Am J Hum Genet 2006;78:1026–1034.
5. Spelbrink JN, Li FY, Tiranti V, et al. Human mitochondrial DNA deletions associated with mutations in the gene encoding Twinkle, a phage T7 gene 4-like protein localized in mitochondria. Nat Genet 2001;28:223–231.
6. Ronchi D, Di Fonzo A, Lin W, et al. Mutations in DNA2 link progressive myopathy to mitochondrial DNA instability. Am J Hum Genet 2013;92:293–300.
7. Kaukonen J, Juselius JK, Tiranti V, et al. Role of adenine nucleotide translocator 1 in mtDNA maintenance. Science 2000;289: 782–785.
8. Nishino I, Spinazzola A, Hirano M. Thymidine phosphorylase gene mutations in MNGIE, a human mitochondrial disorder. Science 1999;283:689–692.
9. Tyynismaa H, Sun R, Ahola-Erkkilä S, et al. Thymidine kinase 2 mutations in autosomal recessive progressive external ophthalmoplegia with multiple mitochondrial DNA deletions. Hum Mol Genet 2012;21:66–75.
10. Tyynismaa H, Ylikallio E, Patel M, et al. A heterozygous truncating mutation in RRM2B causes autosomal-dominant progressive external ophthalmoplegia with multiple mtDNA deletions. Am J Hum Genet 2009;85:290–295.
11. Ronchi D, Garone C, Bordoni A, et al. Next-generation sequencing reveals DGUOK mutations in adult patients with mitochondrial DNA multiple deletions. Brain 2012;135:3404–3415.
12. Garone C, Rubio JC, Calvo SE, et al. MPV17 mutations causing adult-onset multisystemic disorder with multiple mitochondrial DNA deletions. Arch Neurol 2012;69:1648–1651.
13. Luoma P, Melberg A, Rinne JO, et al. Parkinsonism, premature menopause, and mitochondrial DNA polymerase gamma mutations: clinical and molecular genetic study. Lancet 2004;364:875–882.
14. Baloh RH, Salavaggione E, Milbrandt J, Pestronk A. Familial parkinsonism and ophthalmoplegia from a mutation in the mitochondrial DNA helicase twinkle. Arch Neurol 2007;64:998–1000.
15. Bender A, Krishnan KJ, Morris CM, et al. High levels of mitochondrial DNA deletions in substantia nigra neurons in aging and Parkinson disease. Nat Genet 2006;38:515–517.
16. Hudson G, Amati-Bonneau P, Blakely EL, et al. Mutation of OPA1 causes dominant optic atrophy with external ophthalmoplegia, ataxia, deafness and multiple mitochondrial DNA deletions: a novel disorder of mtDNA maintenance. Brain 2008;131:329–337.
17. Amati-Bonneau P, Valentino ML, Reynier P, et al. OPA1 mutations induce mitochondrial DNA instability and optic atrophy 'plus' phenotypes. Brain 2008;131:338–351.
18. Alexander C, Votruba M, Pesch UE, et al. OPA1, encoding a dynamin-related GTPase, is mutated in autosomal dominant optic atrophy linked to chromosome 3q28. Nat Genet 2000;26:211–215.
19. Delettre C, Lenaers G, Griffoin JM, et al. Nuclear gene OPA1, encoding a mitochondrial dynamin-related protein, is mutated in dominant optic atrophy. Nat Genet 2000;26:207–210.
20. Ferré M, Amati-Bonneau P, Tourmen Y, et al. eOPA1: an online database for OPA1 mutations. Hum Mutat 2005;25:423–428.
21. Yu-Wai-Man P, Griffiths PG, Gorman GS, et al. Multi-system neurological disease is common in patients with OPA1 mutations. Brain 2010;133:771–786.
22. Maresca A, la Morgia C, Caporali L, et al. The optic nerve: a "mito-window" on mitochondrial neurodegeneration. Mol Cell Neurosci 2013;55:62–76.
23. Elachouri G, Vidoni S, Zanna C, et al. OPA1 links human mitochondrial genome maintenance to mtDNA replication and distribution. Genome Res 2011;21:12–20.
24. Rouzier C, Bannwarth S, Chaussenot A, et al. The MFN2 gene is responsible for mitochondrial DNA instability and optic atrophy 'plus' phenotype. Brain 2012;135:23–34.
25. Savini G, Carbonelli M, Barboni P. Retinal nerve fiber layer thickness measurement by Fourier-domain optical coherence tomography: a comparison between cirrus-HD OCT and RTVue in healthy eyes. J Glaucoma 2010;19:369–372.
26. La Morgia C, Achilli A, Iommarini L, et al. Rare mtDNA variants in Leber hereditary optic neuropathy families with recurrence of myoclonus. Neurology 2008;70:762–770.
27. Ratiney H, Sdika M, Coenradie Y, et al. Time-domain semi-parametric estimation based on a metabolite basis set. NMR Biomed 2005;18:1–13.
28. Lodi R, Tonon C, Valentino ML, et al. Defective mitochondrial ATP production in skeletal muscle from patients with dominant optic atrophy due to OPA1 mutations. Arch Neurol 2011;68:67–73.
29. Valente EM, Abou-Sleiman PM, Caputo V, et al. Hereditary early-onset Parkinson's disease caused by mutations in PINK1. Science 2004;304:1158–1160.
30. Kitada T, Asakawa S, Hattori N, et al. Mutations in the parkin gene cause autosomal recessive juvenile parkinsonism. Nature 1998;392:605–608.
31. Zanna C, Ghelli A, Porcelli AM, et al. OPA1 mutations associated with dominant optic atrophy impair oxidative phosphorylation and mitochondrial fusion. Brain 2008;131:352–367.
32. Pesch UE, Leo-Kottler B, Mayer S, et al. OPA1 mutations in patients with autosomal dominant optic atrophy and evidence for semi-dominant inheritance. Hum Mol Genet 2001;10:1359–1368.
33. Trounce IA, Kim YL, Jun AS, Wallace DC. Assessment of mitochondrial oxidative phosphorylation in patient muscle biopsies, lymphoblasts, and transmitochondrial cell lines. Methods Enzymol 1996;264:484–509.
34. Porcelli AM, Angelin A, Ghelli A, et al. Respiratory complex I dysfunction due to mitochondrial DNA mutations shifts the voltage threshold for opening of the permeability transition pore toward resting levels. J Biol Chem 2009;284:2045–2052.

35. Robinson BH, Petrova-Benedict R, Buncic JR, Wallace DC. Nonviability of cells with oxidative defects in galactose medium: a screening test for affected patient fibroblasts. Biochem Med Metab Biol 1992;48:122–126.
36. Patergnani S, Marchi S, Rimessi A, et al. PRKCB/protein kinase C, beta and the mitochondrial axis as key regulators of autophagy. Autophagy 2013;9:1367–1385.
37. Klionsky DJ, Abdalla FC, Abeliovich H, et al. Guidelines for the use and interpretation of assays for monitoring autophagy. Autophagy 2012;8:445–544.
38. Patergnani S, Pinton P. Mitophagy and mitochondrial balance. Methods Mol Biol 2015;1241:181–194.
39. Milone M, Younge BR, Wang J, et al. Mitochondrial disorder with OPA1 mutation lacking optic atrophy. Mitochondrion 2009;9: 279–281.
40. Suomalainen A, Majander A, Haltia M, et al. Multiple deletions of mitochondrial DNA in several tissues of a patient with severe retarded depression and familial progressive external ophthalmoplegia. J Clin Invest 1992;90:61–66.
41. Austin SA, Vriesendorp FJ, Thandroyen FT, et al. Expanding the phenotype of the 8344 transfer RNAlysine mitochondrial DNA mutation. Neurology 1998;51:1447–1450.
42. Mancuso M, Ricci G, Choub A, et al. Autosomal dominant psychiatric disorders and mitochondrial DNA multiple deletions: report of a family. J Affect Disord 2008;106:173–177.
43. Hannah-Shmouni F, Sirrs S, Mezei MM, et al. Increased prevalence of hypertension in young adults with high heteroplasmy levels of the MELAS m.3243A>G mutation. JIMD Rep 2014;12:17–23.
44. Agier V, Oliviero P, Lainé J, et al. Defective mitochondrial fusion, altered respiratory function, and distorted cristae structure in skin fibroblasts with heterozygous OPA1 mutations. Biochim Biophys Acta 2012;1822:1570–1580.
45. Ashrafi G, Schwarz TL. The pathways of mitophagy for quality control and clearance of mitochondria. Cell Death Differ 2013;20:31–42.
46. Suen DF, Narendra DP, Tanaka A, et al. Parkin overexpression selects against a deleterious mtDNA mutation in heteroplasmic cybrid cells. Proc Natl Acad Sci U S A 2010;107:11835–11840.
47. White KE, Davies VJ, Hogan VE, et al. OPA1 deficiency associated with increased autophagy in retinal ganglion cells in a murine model of dominant optic atrophy. Invest Ophthalmol Vis Sci 2009; 50:2567–2571.
48. Sarzi E, Angebault C, Seveno M, et al. The human OPA1delTTAG mutation induces premature age-related systemic neurodegeneration in mouse. Brain 2012;135:3599–3613.
49. Narendra D, Walker JE, Youle R. Mitochondrial quality control mediated by PINK1 and Parkin: links to parkinsonism. Cold Spring Harb Perspect Biol 2012;4.
50. Corti O, Brice A. Mitochondrial quality control turns out to be the principal suspect in parkin and PINK1-related autosomal recessive Parkinson's disease. Curr Opin Neurobiol 2013;23:100–108.
51. Marongiu R, Ferraris A, Ialongo T, et al. PINK1 heterozygous rare variants: prevalence, significance and phenotypic spectrum. Hum Mutat 2008;29:565.
52. Müller-Rischart AK, Pilsl A, Beaudette P, et al. The E3 ligase parkin maintains mitochondrial integrity by increasing linear ubiquitination of NEMO. Mol Cell 2013;49:908–921.
53. Lutz AK, Exner N, Fett ME, et al. Loss of parkin or PINK1 function increases Drp1-dependent mitochondrial fragmentation. J Biol Chem 2009;284:22938–22951.